ACS APPLIED MATERIALS & INTERFACES

www.acsami.org Research Article

Atom-Vacancy-Defect-Derived Electric Hysteresis Loops and Stochastic Low-Frequency Noises in Few-Atom Layer MoS_2

Mioko Kosugi, Shunta Furuichi, Yung-Chang Lin, Yusuke Kobayashi, Keita Takaki, Takashi Kikkawa, Takashi Taniguchi, Kenji Watanabe, Takashi Kohno, Kazu Suenaga, Eiji Saitoh, Shigeo Maruyama, and Junji Haruyama*

Cite This: https://doi.org/10.1021/acsami.4c13147 Read Online

ACCESS | Metrics & More | Article Recommendations | Supporting Information

Downloaded via Junji Haruyama on November 6, 2024 at 01:49:44 (UTC).
See https://pubs.acs.org/sharingguidelines for options on how to legitimately share published articles.

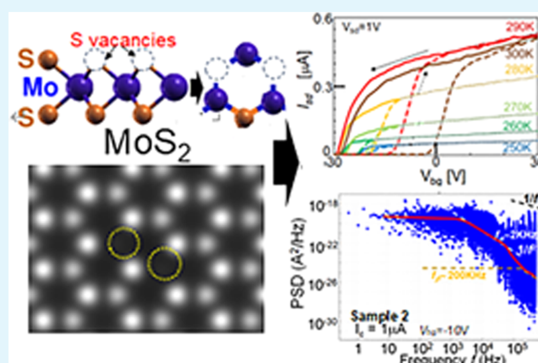

ABSTRACT: Atom-vacancy-defects present in various materials yield numerous interesting physical phenomena, even obstructing high performance in some cases. On the other hand, their valuable applications to novel devices, such as nitrogen vacancy centers in diamond for quantum bits, have gathered significant attention. In particular, these tendencies become more substantial in two-dimensional (2D) (atomically) thin van der Waals layers. However, correlations with various kinds of atom defects are still under exploration. Herein, we find the stochastic behaviors of large hysteresis loops with strong photoresponse in the static electrical properties in few-atom layer semiconductors, molybdenum disulfide (MoS_2). The temperature dependence and transmission electron microscopy reveal that they arise from pairs of two neighboring in-plane S-vacancy defects, which predominantly present only around the interface at the MoS_2 flake/substrate, with activation energies ~0.35 eV. The low-frequency (f) (LF) noise measurements clarify a high f shift in the two $1/f^2$-dependent regimes, implying stochastic behaviors of electric charges through the S-vacancy pairs with high-speed charge(spin) transitions across low kinetic energy barriers between narrow discrete states. The shallow energy sates are formed from the highly uniform S-vacancy pairs interacting with Mo atoms, which act like quantum dots. The observed stochastic operation holds promise for various application, particularly for probabilistic neuromorphic computation in artificial intelligence.

KEYWORDS: *defects, atom vacancy, few-atom layer van der Waals semiconductors, hysteresis loop, low-frequency noise, stochastic charge behaviors, quantum dots*

INTRODUCTION

The physical behaviors derived from atom-vacancy defects and their applications in highly efficient electronic and photonic devices are gathering substantial attention in two-dimensional (2D) (atomically) thin van deer Waals (vdW) semiconductors (e.g., the transition-metal dichalcogenide (TMDC) family like molybdenum disulfide (MoS_2)), as even few atom-vacancy defects drastically alter those physical properties. Various types of atom-vacancy defects have been identified in these materials (e.g., surfer (S) vacancies in MoS_2; Figure 1a−c).[1−6] These defects result in various defect-derived midgap states with different activation energies (E_a) and electric behaviors. S vacancies have the lowest formation energies and are the most stable from chemical and thermal respect viewpoints in MoS_2 layers.[2]

Various methods have been employed to investigate the physical properties arising from defects (Supporting Information SI 1),[7−16] e.g., photoluminescence (PL), high-resolution transmission electron microscopy (HRTEM), deep-level transient spectroscopy (DLTS), and low-frequency (f) (LF) noises.[11−16] Of particular note, a previous study revealed that the S vacancies like Figure 1a,b produced a deep level with E_a ~ 0.6 eV in MoS_2 layers, while those like Figure 1c,d led to various shallow E_a ~ 0.2−0.4 eV.[1,2] The observation of PL in the presence of mono S vacancies with magnetic fields also elucidated some defect-derived midgap energy states and defect−defect (-band edge) charge (or spin) transitions, implying even zero-field spin splitting of degenerated defect-spin states by spin−orbit interactiona.[7] These findings suggest the possibility that atom vacancies in the TMDC family act similarly to nitrogen vacancy (NV) centers in diamond.[17−19]

Moreover, measurements of LF noises originating from even a mono S vacancy revealed a $1/f^2$ dependence instead of the typical $1/f$ dependence (SI 1).[11] This suggested that the mono

Received: August 5, 2024
Revised: October 15, 2024
Accepted: October 28, 2024

© XXXX American Chemical Society

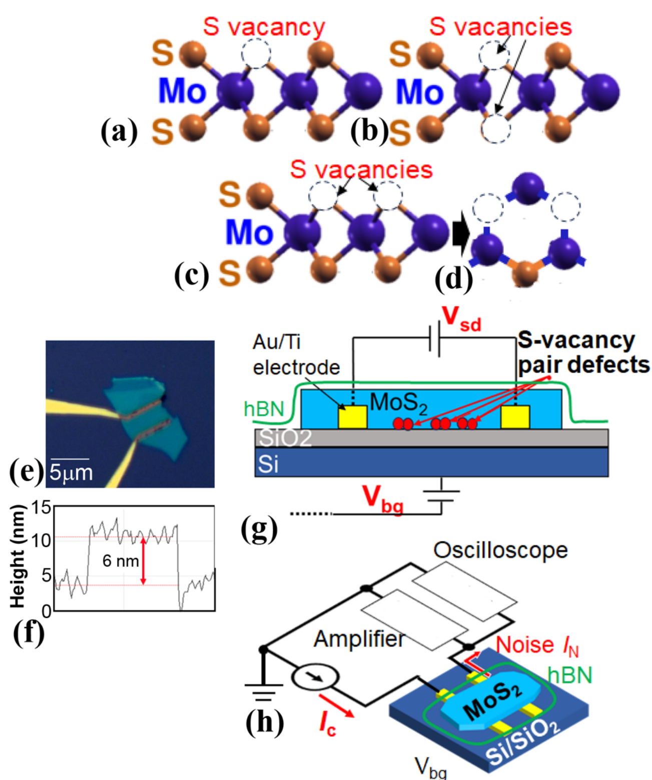

Figure 1. Schematic views of crystal structures and measurement methods and sample characterization. (a−c) Schematic cross-sectional views of three types of S vacancies in a monoquantum layer of MoS_2, (d) top view of (c), (e) example of an optical microscope image showing a few-atom layer MoS_2 flake attached to prefabricated two Au/Ti electrodes on a SiO_2/Si substrate (without a hBN cover layer only for this image), fabricated using vdW mechanical exfoliation of bulk material with Scotch tapes and PDMS sheet transfer technique (SI 2). (f) Cross-sectional AFM image of (e), schematic views of (g) sample cross section for DC electrical measurements and (h) LF noise measurements. V_{sd} and V_{bg} are applied between the two electrodes and from the sample back side, respectively, in (g). Noise current (I_N) is measured using an oscilloscope at room T, while changing I_c and V_{bg} in (h).

S vacancy introduces new electronic states within the bandgap and discrete energy states, resulting in charge switching responsible for LF noises. These findings clarified the possibility that S vacancies with neighboring Mo atoms act like quantum dots providing precise discrete states, leading to stochastic behaviors.[20−26]

Defects in TMDC semiconductors can be also introduced by various methods, e.g., electron, laser, ion (Ar, He), and X-ray beam irradiations, as well as the attachment of TMDC flakes onto SiO_2/Si substrates, and the fabrication of metal electrodes on TMDC flakes.[27−29] Indeed, we have uncovered unique physical properties resulting from defects in thin MoS_2 flakes induced by electron-[27] and laser-beam (LB)[28,29] irradiations. These irradiations triggered a phase transition from semiconducting to metallic phases, creating 1D lateral Schottky junctions at the interface between them. This led to the emergence of various defects, particularly with LB irradiation, which caused an abundance of defects due to heat diffusion.[28,29] It was revealed that such defects caused a rise in unique hysteresis loops in current−voltage relationships, resulting from the capture and emission of electrical charges (electron and holes) depending on the applied voltage bias and the holding times.[29] Nevertheless, detailed correlations of various atom-vacancy defects with static and dynamic behaviors are still under exploration.

In the present research, we explore the static electronic and photonic properties, as well as the dynamic behaviors (LF noises) resulting from atom-vacancy defects in vdW few-layer MoS_2 flakes roofed by hexagonal boron-nitride (hBN) layers. The stochastic behaviors of the large hysteresis loops with strong photoresponse are found in the current vs back gate voltage (V_{bg}) curves, applied from the back side of the substrate, disclosing the presence of defects only around the junction interface of the MoS_2 flake/(the SiO_2/Si substrate). Their temperature (T) dependence and HRTEM observation suggest that the hysteresis loops are yielded from predominantly existing pairs of two neighboring in-plane S vacancies (Figure 1c,d) with $E_a \sim 0.35$ eV. The measurements of LF noise (noise currents (I_N) and noise power spectrum density (PSD)) clarify the high f shift observed in the two $1/f^2$-dependent regimes, indicating stochastic behaviors of electric charges via the S-vacancy pairs producing the large hysteresis curves with fast transitions across a few meV kinetic energy barriers between narrow discrete states, created from spin interactions in the parallel coupling of the two S vacancies. The observed PSD behaviors suggest the possibility that the coupled two S vacancies (with high uniformity) interacting with Mo atoms deliver electronic states similar to those found in quantum dots, despite the measurements of many S-vacancy pairs at room T.

EXPERIMENTAL SECTION

Materials and Characterization. For the present research, vdW-fabricated few-layer MoS_2 flakes (the thickness ∼6 nm), roofed by high-quality hBN layers, have a current flow area ∼3 × 5 μm^2 with $\sim 10^5$ defects between two Au/Ti electrodes (Figure 1e−1g) (SI 2). Few-layer MoS_2 flakes are affixed onto prefabricated two Au/Ti electrodes placed on the SiO_2/Si substrate through mechanical exfoliation of bulk MoS_2 (purchased from hq Graphene Co.) using Scotch tapes and poly dimethylsiloxane (PDMS) sheets (Figure 1e), employing a 2D heterostructure transfer system (HQ graphene Co.) after plasma cleaning the surface of the SiO_2/Si substrate for as long as 30 min under high vacuum. When assuming a defect density of $\sim 10^{12}$ cm^{-2} in conventional MoS_2, there are $\sim 10^5$ defects present over this current flow area. The thickness of ∼6 nm was confirmed by using atomic force microscopy (Figure 1f) and Raman spectroscopy. Following the formation, each sample is covered by a high-quality hBN monolayer. All processes are conducted within a glovebox under an Ar gas atmosphere.

RESULTS AND DISCUSSION

DC Measurements and Hysteresis Curves. Figure 2 exhibits typical two-probe source−drain current (I_{sd}) vs source−drain voltage (V_{sd}) (Figure 2a) and I_{sd} vs V_{bg} curves, applied from the back side of the substrate, (Figure 2b−d) relationships at room T (Figure 1g) (SI 2). Despite the 3-fold measurements conducted under light and dark ambient conditions at V_{bg} = 0 V, Figure 2a suggests the absence of hysteresis loops. This result indicates the absence of defects at the interface around the MoS_2 and Au/Ti electrodes, as well as around the MoS_2 surface interfacing with the hBN cover layer. This is because hysteresis loops in the I_{sd}−V_{sd} relationships are conventionally caused from the capture and emission of electric charges through defects (Figure 5), which are triggered by varying V_{sd}. The applied V_{bg} of 0 V also leads to a strong interaction of the I_{sd} flow with the surface-side defects as

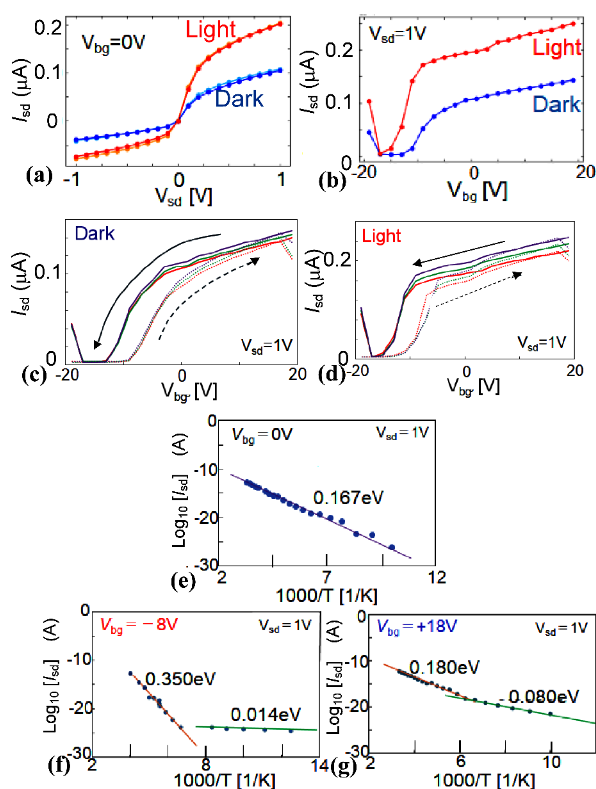

Figure 2. Basic DC electrical properties of a few-layer MoS_2 flake with small hysteresis loops (sample 1) (a−d). Typical measurement results for (a) $I_{sd}-V_{sd}$ curve at fixed V_{bg} = 0 V and (b−d) $I_{sd}-V_{bg}$ curve at fixed V_{sd} = +1 V with three sets of measurements (except for (b)) conducted under light and dark ambient conditions at room T. Arrows in parts (c and d) indicate the directions for V_{bg} sweep. Typical T dependence of I_{sd} for the sample described in figure 2c, presented as Arrhenius plots for three different V_{bg} regions (e−g). (e) V_{bg} = 0, V_{bg} regions corresponding to (f) appearance and (g) disappearance of the hysteresis loop.

opposed to a weak interaction with the substrate-side defects. The high-quality hBN layer covering the surface prevents surface oxidization and the appearance of oxygen-based defects. Moreover, attaching MoS_2 flakes onto the prefabricated Au/Ti electrodes reduces defects existing at the electrodes/MoS_2 interface.

On the other hand, small hysteresis loops are confirmed in the region under both light and dark ambient conditions, as shown in Figure 2c,d, when $-V_{bg}$ is applied at room T. Particularly noteworthy is the instability observed in Figure 2d across three sets of measurements. These results strongly suggest the presence of defects at the interface around MoS_2 and the SiO_2/Si substrate because varying V_{bg} causes a strong interaction of I_{sd} with the substrate-side defects. V_{bg}-triggered capture and emission of the electric charges through the defects lead to the observed hysteresis loops (Figure 5). Especially, the observed instability under light conditions (Figure 2d) suggests the possibility of stochastic behaviors in the emission and capture of electric charges. Additionally, the increase in I_{sd} for the $+V_{bg}$ regions indicates that the MoS_2 flakes exhibit n-type semiconductor behavior.

***T* Dependence Associated with Hysteresis Loops and Activation Energies.** The T dependence of I_{sd} for three different V_{bg} regions, distinguished by the magnitudes of the hysteresis loops (V_{bg} = +18, 0, −8 V) in Figure 2c, is presented in Figure 2e−g in the form of an Arrhenius plot (SI 2). For region 1, showing no hysteresis loops (Figure 2g), a shallow E_a level ∼0.08 eV and a middle E_a level ∼0.18 eV are confirmed above and below $1000/T$ ∼ 6, respectively. Region 2 (Figure 2e), presenting a small hysteresis loop, shows only one middle level E_a ∼ 0.167 eV. In contrast, region 3, exhibiting larger hysteresis loops (Figure 2f), displays a shallow E_a ∼ 0.014 eV and a deeper level E_a ∼ 0.35 eV above and below $1000/T$ ∼ 7, respectively. These E_a levels can be compared with those in a previous DFT calculation as follows.[2]

The shallow E_a levels ∼ 0.08 eV in region 1 and ∼0.014 eV in region 3 are close to the E_a calculated from the Mo-interlayer vacancy.[2] The middle E_a levels ∼0.18 eV in region 1 and ∼0.167 eV in region 2 are approximately close to the E_a calculated from the Mo vacancy.[2] These states exist independently from the presence of the hysteresis loop and thus do not contribute to the formation of hysteresis loops at room T. This is because such Mo-based defects need much higher formation energies (e.g., ∼7 eV for Mo-interlayer and ∼4 eV for Mo vacancy as the maximum cases) compared with S-based defects (∼2 eV), (2) leading to significantly small densities. Conversely, the deeper E_a level ∼ 0.35 eV in region 3 is close to the E_a calculated from the S vacancy.[2] Since this level is only confirmed in region 3, it suggests that the hysteresis loop originates from this deeper level arising from the S vacancy, possibly with a high density.

Figure 3a depicts the T dependence of $I_{sd}-V_{bg}$ curves in another sample (sample 2), which presents hysteresis loops significantly larger than that of Figure 2 at room T. The V_{bg} range presenting the hysteresis loop at room T drastically broadens, extending even to the V_{bg} range between ∼−30 and 0 V. The hysteresis loop diminishes rapidly as T decreases. Arrhenius plots illustrating the T dependence of I_{sd} below $1000/T < 4$ in three different V_{bg} regions, distinguished by the magnitudes of the hysteresis loops, are shown in Figure 3b−d. The observed E_a ∼ 0.34−0.35 eV across all V_{bg} regions are almost consistent and akin to the deeper level E_a ∼ 0.35 eV observed in region 3 (Figure 2f). This strongly advocates that the presence of the S vacancy introduces the observed large hysteresis loops into $I_{sd}-V_{bg}$ relationships. A summary of the confirmed E_a values in the two samples is provided in SI 3, further elucidating the aforementioned explanation.

Moreover, another DFT calculation, which was compared with DLTS measurements and HRTEM observation, also reported E_a ∼ 0.35 eV originating from two neighboring in-plane S-vacancy pairs (Figure 1c).[1] Indeed, examples of HRTEM images of the MoS_2 monolayer reveal the presence of many S-vacancy pairs (Figure 3e−g). Consequently, the observed hysteresis loops in the $I_{sd}-V_{bg}$ relationships can be primarily attributed to the pairs of two neighboring in-plane S vacancies. Because the S vacancy needs the lowest formation energy in MoS_2, this is the most stable from both chemical and thermal viewpoints,[2] leading to high defect density. The reason why this E_a is independent of the magnitude of the hysteresis loops (i.e., regions in V_{bg}) in Figure 3a−d while only region 3 presents this deeper E_a in Figure 2f will be discussed later.

LF Noise Observation. Dynamic behaviors (LF noises) associated with these S-vacancy pairs measured at room T are presented in Figure 4, showing examples of the noise currents (I_N) and noise PSD in the samples with small (Figure 4a,b) and large (Figure 4c,d) hysteresis loops (i.e., Figures 2 and 3 samples, respectively) at V_{bg} where the hysteresis loops are observed (Figure 1h) (SI 2). As prefixed DC currents (I_c)

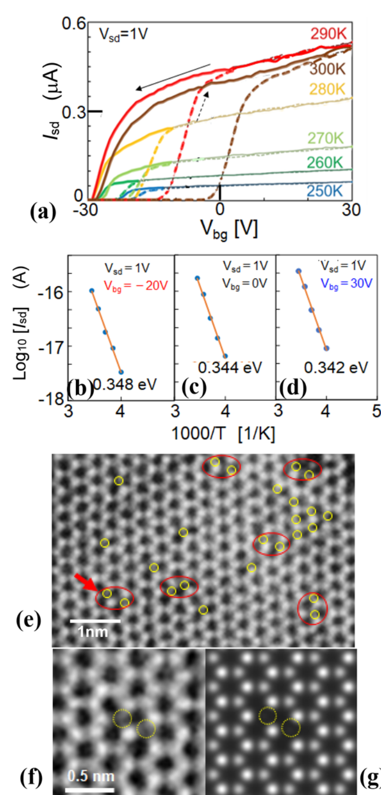

Figure 3. T-dependence of the I_{sd}−V_{bg} curve in sample 2 with larger hysteresis loops (a−d). (a) Each curve color corresponds to a different T. Solid and dotted arrows indicate the directions for V_{bg} sweep for all curves. (b−d) Typical T dependence of I_{sd} presented as Arrhenius plots for three different V_{bg} regions in (a). (c) V_{bg} = 0, V_{bg} regions corresponding to (b) appearance and (d) disappearance of the hysteresis loops. I_{sd} values for the upper parts of the hysteresis loops are employed. Examples of top-view HRTEM images of another monolayer MoS_2 (e−g). (e) Yellow circles correspond to single S vacancies, while red circles surrounding two yellow circles represent isolated pairs of two neighboring S vacancies. (f) Higher resolution image of the S-vacancy pair indicated by the red arrow in (e). Two yellow dotted circles indicate two neighboring S vacancies along the monolayer, corresponding to Figure 1c,d. (g) Simulation image of (f). Brighter white and dark dots correspond to Mo and S atoms, respectively.

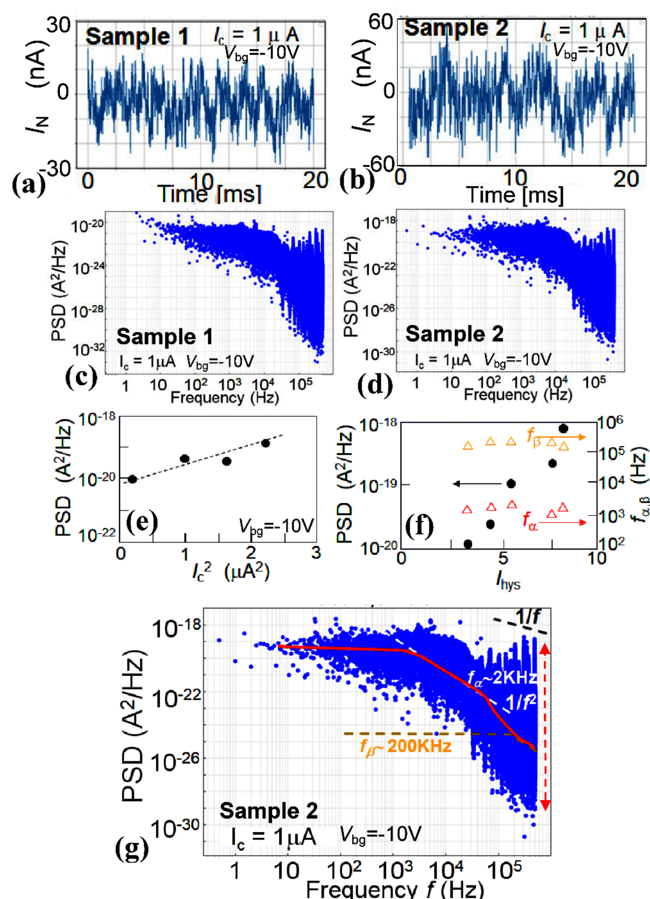

Figure 4. LF noise measurement results of samples 1 and 2 with the small and large hysteresis loops, respectively, at room T. (a, b) I_N and (c, d) PSD under a constant I_c. (e, f) PSD values as a function of I_c^2 (e) and I_{hys} (f) at $f = 1.5 \times 10^2$ Hz. For (f), PSD values (black circles) are shown on the left Y-axis, while f_α and f_β values (red and orange triangles, respectively) are also presented on the right Y-axis. I_{hys} represents the maximum amplitude I of each hysteresis loop, determined from the I_{max}/I_{min} at each V_{bg} which shows the largest loop in each I_{sd}−V_{bg} hysteresis curve, including sample 1. (g) Typical data fit by eq 1 (red solid curve) of sample 2. White, yellow, and black dotted lines represent $1/f^2$ and $1/f$ dependence on f.

increase, the magnitude of I_N monotonically increases in both samples (SI 4). On the other hand, the PSD behaviors are markedly different from those reported for the mono S vacancy (Figure 4c,d).[11] The f-ranges of the PSD shift to higher regions (i.e., from $f \sim 1{-}10^3$ Hz order for the S monovacancy to $f \sim 10^3{-}10^5$ Hz order in the present S-vacancy pair's case), and the PSD distribution in the high f region increases (i.e., from one to five log-scale orders; indicated by the red dotted arrow along the Y-direction in Figure 4g) in the present results. The PSD amplitude increases in the LF range ($f \sim 10^{10}$ Hz) in both samples as I_c increases (SI 4), revealing a linear I_c^2-dependence for the PSD amplitude (Figure 4e).

Notably, in Figure 4c,d, for the sample with a large hysteresis loop, both the magnitudes of I_N and PSDs are significantly larger than those shown in Figure 4a,b for the sample with a small hysteresis loop. This trend is more evidently illustrated in Figure 4f. These results imply a strong association between the observed I_N and PSD and the stochastic behaviors (capture and emission) of electric charges through the two S-vacancy defects because larger hysteresis loops originate from the presence of a larger number of S-vacancy pairs. Indeed, $1/f$ noise (flicker noise) with a Hooge parameter, which arises not from the stochastic charge behaviors through defects but mainly from the fluctuation of electric charge (mobility) due to scattering by impurities (or defects, lattices, and electrodes),[12−16] is not observed in our measurements (the black dotted line shown in Figure 4g); nevertheless, contact resistance R_c is as high as ∼250 KΩ (SI 5). Moreover, the linear I_c^2-dependence of the PSD amplitude observed in Figure 4e supports the stochastic behaviors of charges (i.e., charge switching among defect states) through the S vacancies following eq 1 as discussed later.

DISCUSSION

Charge Carrier Traps and Emission Sensitive to Changes in V_{bg} and Temperature. Here, we discuss the correlation among the hysteresis loops in the I_{sd}−V_{bg} curves, S-vacancy defects, E_a values, and dynamic behaviors. The E_a values are highly sensitive to the three V_{bg} regions in sample 1, presenting $E_a \sim 0.35$ eV only in V_{bg} region 3 where the small

https://doi.org/10.1021/acsami.4c13147
ACS Appl. Mater. Interfaces XXXX, XXX, XXX−XXX

hysteresis loop opens at room T (Figure 2g), while $E_a \sim 0.35$ eV was confirmed even in the $+V_{bg}$ region where the large hysteresis loop closes in sample 2 (Figure 3d). This result arises from different sensitivities of the charge carrier traps to the defect states concerning changes in V_{bg} at room T and changes in T.

When $+V_{bg}$ is applied at room T, electrons are injected into the present n-type MoS_2, and the defect energy states ($E_a \sim 0.35$ eV) formed from the two coupled S vacancies are fully occupied by these electrons (Figure 5a). As V_{bg} is swept from

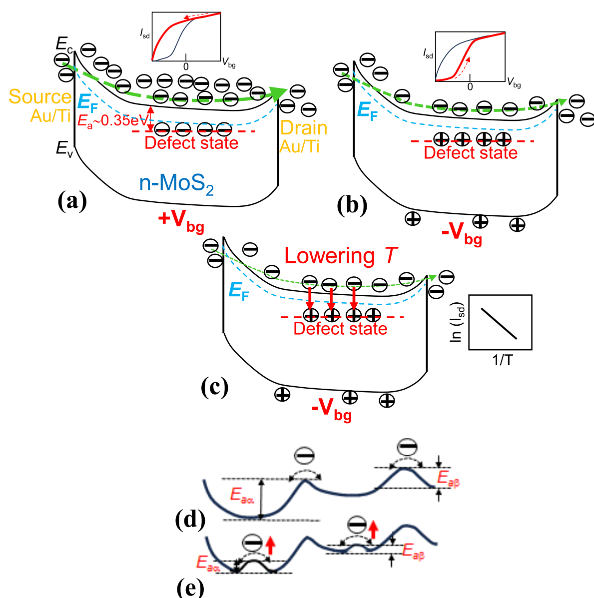

Figure 5. (a−c) Schematic views of band diagrams illustrating capture and emission of electrons through defect states arising from the two S vacancies coupled in parallel, corresponding to three different V_{bg} regions and each part of the hysteresis loop in Figures 2c,d and 4a (insets of a, b) and T dependence (inset of c). (d, e) Schematic potential views depicting charge (spin) transitions leading to LF noises for (d) mono S vacancy (Figure 1a) and (e) two S vacancies coupled in parallel with smaller E_a (Figure 1c,d).

$+V_{bg}$ to $-V_{bg}$, these accumulated electrons are gradually emitted from the defect states, and the states become empty in the largest $-V_{bg}$ region (Figure 5b). When V_{bg} is swept back from this $-V_{bg}$ to $+V_{bg}$, I_{sd} becomes smaller than that that for the abovementioned V_{bg} sweep (i.e., from $+V_{bg}$ to $-V_{bg}$) because the defect states are empty, resulting in the appearance of the hysteresis loop. As V_{bg} is further swept to the $+V_{bg}$ region, the defect states are gradually occupied by injected electrons, and then the hysteresis loop entirely closes in the largest V_{bg} region due to the fully occupied defect states, similar to the initial condition.

On the other hand, the T dependence of I_{sd}, leading to the observation of E_a, is caused by the occupation of the empty defect states (at room T) by electrons, as T decreases (Figure 5c). The result observed in Figure 2f for the open hysteresis loop is consistent with this explanation, while that in Figure 3d for the closed loop seems to be inconsistent. This implies that some defect states are still empty even at room T in this $+V_{bg}$ region (Figure 3d) despite the closed loops (Figure 3a), and thus electrons can be partially captured by such empty states with decreasing T. Because The Figure 3-sample presents a larger hysteresis loop, the number of two S-vacancy pairs (Figure 3e−g) should be considerably larger than those in the Figure 2-sample. Thus, this means that the different probabilities of electron capture by the empty defect states between the V_{bg} sweep (for the closure of the hysteresis loops) at room T and the T decrease. When T reduction has a capture probability higher than that of the V_{bg} sweep, even remaining empty states, which cannot be occupied by electron injection due to the V_{bg} sweep at room T, can capture electrons, resulting in the observation of E_a. Otherwise, the sensitivity of the $I_{sd}-V_{bg}$ hysteresis loops to electron capture by defect states may not be sufficient.

Correlation between LF Noises and In-Plane S-Vacancy Pairs for High-Speed Charge Transition. Ref 11 measured LF noises arising solely from the S monovacancy using a conductive AFM with a probe radius <25 nm, where only mono S vacancies can be included. In contrast, we have measured an area $\sim$15 μm^2 of MoS_2 flakes between two electrodes, where defects with a number $<\sim 10^5$ may exist. Electron(mobility) fluctuation, which basically arises from scattering by impurities (or defects, lattices, and electrodes), conventionally dominates as the origin for LF noises for such field-effect transistor structures, resulting in $1/f$ noise.[11−16] However, $1/f$ noise (the black dotted line in Figure 4g) is not confirmed in our samples, as mentioned earlier (SI 5). Moreover, the LF noises highly depend on the magnitude of the hysteresis loops arising from the S-vacancy pairs (Figure 4f). These results strongly suggest that stochastic behaviors (capture and emission or state switching) of electric charges through only the S-vacancy pairs can be the dominant causes for the observed PSDs despite the large area measurements, implying that many in-plane S-vacancy pairs predominantly exist with high uniformity among various defects. Indeed, many S-vacancy pairs are confirmed in Figure 3e−g, although the density depends on the observed area. The S vacancy has the lowest formation energy ($\sim$2 eV),[2] while the reason for the predominant existence of the S-vacancy pairs in the present samples, rather than isolated mono S vacancies, may be associated with our fabrication method (SI 6).

The observed PSD behaviors associated with the S-vacancy pairs are markedly different from those reported for the mono S vacancy.[11] The observed f-ranges of the PSD shift to higher f regions, and the PSD amplitude at the high f region increases in the present results. Moreover, the best data fit using eq 1 (red solid curve in Figure 4g), utilizing two Lorentzian functions provided in ref 11, evidently reveals the two $(1/f)^2$-proportional regions following eq 1 with $f_\alpha \sim 2$ kHz (white dotted line) and $f_\beta \sim 200$ kHz (yellow dotted line).

$$S_I(f) = \frac{A_\alpha(I_{bias})I_{bias}^2}{1 + \left(\frac{f}{f_\alpha}\right)^2} + \frac{A_\beta(I_{bias})I_{bias}^2}{1 + \left(\frac{f}{f_\beta}\right)^2} + C \tag{1}$$

$$\tau(T) = \frac{1}{2\pi f(T)} = \frac{1}{\sigma^{(0)} \times \exp\left(\frac{-E}{k_B T}\right) \times N_T \times \nu} \tag{2}$$

where $I_{bias} = I_c$; A_α and A_β are the amplitudes of the Lorentzian functions of widths at f_α and f_β, respectively; and C represents a flat background describing the measured system noise spectrum for eq 1, and with the high-T limit capture cross-section $\sigma(0)$, the kinetic barrier E between discrete states, the trap state density per unit volume N_T, and the electron velocity ν for eq 2.

https://doi.org/10.1021/acsami.4c13147
ACS Appl. Mater. Interfaces XXXX, XXX, XXX−XXX

For regions (1), the observed f_α and f_β values are ~500-times and 200-times faster than $f_\alpha \sim 4$ Hz and $f_\beta \sim 1.2$ kHz estimated for the mono S vacancy, respectively,[11] and are almost independent of I_{hys} (Figure 4f). The T-dependence of these f_α and f_β for the S monovacancy provided $E_{a\alpha} \sim 15$ and $E_{a\beta} \sim 23$ meV, respectively, by the best data fit using Shockley−Read−Hall (SRH) statistics eq (eq 2).[11] These E_a values were interpreted as the two kinetic energy barriers between the three discrete defect states formed from the mono S vacancy, leading to the charge transition over the E_a (Figure 5d).

Based on these previous findings, the observed shift of the PSDs to higher f ranges with higher f_α and f_β values indicates the faster charge transition over narrower discrete energy states (lower E_a) (Figure 5e). From $f_\alpha \sim 2$ kHz and $f_\beta \sim 200$ kHz, $E_{a\alpha} \sim 1.5$ meV and $E_{a\beta} \sim 3$ meV are estimated, respectively, simply assuming values for $N_T \sim 10^{12}/\text{cm}^2$, a tunneling electron velocity, $\nu \sim 10^7$ cm/s, and the absolute scattering cross-section values, $\sigma^{(0)}{}_\alpha \sim 10^{-23}$ cm^2 and $\sigma^{(0)}{}_\beta \sim 10^{-20}$ cm^2, as previously reported.[11] These E_a values, ~10-times smaller than those for the S monovacancy, can be formed by spin (orbit) interactions in the parallelly coupled two neighboring S vacancies with Mo atoms, similar to those for the coupled two quantum dots, even at room T (Figure 5e).[20−26]

As mentioned in the Introduction, indeed, previous PL observation of even mono S-vacancy defects reported zero-field spin−orbit-interaction-derived spin splitting of the degenerated intergap S-vacancy states, evidencing the presence of such small E_a values (~3 meV) with the defect−defect spin transition among those.[7] The f_α and f_β values are almost independent of I_{hys}, although the PSD magnitude linearly depends on I_{hys} (Figure 4f). These indicate that the $E_{a\alpha}$ and $E_{a\beta}$ values are nearly uniform despite being formed from many coupled S-vacancy pairs (Figure 3e−g), suggesting their high uniformity.

S-Vacancy Pairs Interacting Mo Atoms as Quantum Dots. This result also suggests the possibility that the coupled two S vacancies interacting nearby Mo atoms act like quantum dots (possibly like the NV centers of diamond),[17−19] when single electrons are injected at low T (SI 7). The $1/f^\gamma$ (charge or spin) noises have been actually discussed in single or coupled various semiconductor quantum dots (e.g., reporting $0 < \gamma < \sim 2$).[20−26] In particular, it was revealed in InGaAs quantum dots that the low-magnitude spin noise spectrum at high f was purely Lorentzian, falling as $1/f^2$, and the total spectrum collapsed rapidly with f becoming insignificant above 50 kHz.[20] These spin and total noise behaviors are qualitatively similar to ours, thus supporting the notion that spin noises arising from the spin transition in the S-vacancy pairs can contribute to the present LF noises, despite the measurements being conducted on different materials with larger number of defects at room T.

CONCLUSIONS

In summary, we have presented the static physical properties resulting from vacancy defects in vdW few-atom layer MoS_2 flakes along with their dynamic behaviors (LF noises). We have found that stochastic behaviors of the large hysteresis loops in the I_{sd} vs V_{bg} curves originated from the predominant presence of pairs of neighboring in-plane S vacancies, locating only on the substrate surface side. A high-f shift observed in the stochastic LF noises in the two $1/f^2$-dependent regimes has indicated rapid charge (spin) switching across low-energy barriers between narrow discrete states created from the highly uniform S-vacancy pairs interacting with Mo atoms, which may behave like quantum dots. The observed stochastic behaviors of LF noises resulting from the S-vacancy pairs hold promise for the application to probabilistic neuromorphic computation in artificial intelligence, which directly mimics the probabilistic operation of the human brain (SI 8),[30−32] provided that one could control the number and electronic states of the defects and their interactions.

ASSOCIATED CONTENT

Supporting Information

The Supporting Information is available free of charge at https://pubs.acs.org/doi/10.1021/acsami.4c13147.

Background for the research associated with defects; methods for the sample fabrication and measurements; summary of the observed E_a; I_c-dependence of the LF noises; contact resistance and absence of $1/f$ noise; reason for predominant existence of S-vacancy pairs; S vacancy as a quantum dot; and application to neuromorphic computation (PDF)

AUTHOR INFORMATION

Corresponding Author

Junji Haruyama − *Faculty of Science and Engineering, Aoyama Gakuin University, Sagamihara, Kanagawa 252-5258, Japan; Institute for Industrial Sciences, The University of Tokyo, Tokyo 153-8505, Japan;* orcid.org/0000-0003-4793-6968; Email: J-haru@ee.aoyama.ac.jp

Authors

Mioko Kosugi − *Faculty of Science and Engineering, Aoyama Gakuin University, Sagamihara, Kanagawa 252-5258, Japan*

Shunta Furuichi − *Department of Electrical Engineering and Information Systems, The University of Tokyo, Tokyo 153-8505, Japan*

Yung-Chang Lin − *National Institute of Advanced Industrial Science and Technology (AIST), Tsukuba 305-8565, Japan*

Yusuke Kobayashi − *Faculty of Science and Engineering, Aoyama Gakuin University, Sagamihara, Kanagawa 252-5258, Japan*

Keita Takaki − *Faculty of Science and Engineering, Aoyama Gakuin University, Sagamihara, Kanagawa 252-5258, Japan*

Takashi Kikkawa − *Department of Applied Physics, The University of Tokyo, Tokyo 113-8656, Japan*

Takashi Taniguchi − *Research Center for Electronic and Optical Materials, National Institute for Materials Science, Tsukuba 305-0044, Japan;* orcid.org/0000-0002-1467-3105

Kenji Watanabe − *Research Center for Materials Nanoarchitectonics, National Institute for Materials Science, Tsukuba 305-0044, Japan;* orcid.org/0000-0003-3701-8119

Takashi Kohno − *Institute for Industrial Sciences, The University of Tokyo, Tokyo 153-8505, Japan*

Kazu Suenaga − *The Institute of Scientific and Industrial Research, Osaka University, Osaka, Ibaraki 567-0047, Japan*

Eiji Saitoh − *Department of Applied Physics and Institute for AI and Beyond, The University of Tokyo, Tokyo 113-8656, Japan; WPI Advanced Institute for Materials Research, Tohoku University, Sendai 980-8577, Japan; Advanced Science Research Center, Japan Atomic Energy Agency, Naka-gun, Ibaraki 319-1195, Japan*

Shigeo Maruyama – *Department of Mechanical Engineering, The University of Tokyo, Tokyo 113-8656, Japan;* orcid.org/0000-0003-3694-3070

Complete contact information is available at:
https://pubs.acs.org/10.1021/acsami.4c13147

Author Contributions

M.K. and J.J. conceived and designed the experiment. C.T., K.K., M.K., and S.F. carried out the experiments with the help of T.K. and E.S. Y.-C.L. and K. S. performed the sample characterization using HRTEM. T.T. and K. W. provided the high-quality hBN crystals. K.S., S.M., K.H., and J.H. supervised the research and experiments.

Funding

The work at the Aoyama Gakuin University was partly supported by the Aoyama Gakuin University Research Institute grant program for the creation of innovative research. Work at the University of Tokyo was partly supported by JSPS KAKENHI (Grant Numbers JP21KK0087, JP23H00174, and JP23H05443) and by JST, CREST (Grant Number JPMJCR20B5, Japan) for S.M. and JST-CREST (JPMJCR20C1 and JPMJCR20T2), Grant-in-Aid for Scientific Research (JP19H05600 and JP24K01326) and Grant-in-Aid for Transformative Research Areas (JP22H05114) from JSPS KAKENHI, MEXT Initiative to Establish Next-Generation Novel Integrated Circuits Centers (X-NICS) (JPJ011438), Japan, and Institute for AI and Beyond of the University of Tokyo for T.K. and E.S. K.W. and T.T. acknowledge support from the JSPS KAKENHI (Grant Numbers 20H00354, 21H05233, and 23H02052) and the World Premier International Research Center Initiative (WPI), MEXT, Japan.

Notes

The authors declare no competing financial interest.

■ ACKNOWLEDGMENTS

We thank K.H., S.M., Y.Y., T.A., A.H.M., J.J.P., R.W., and P.K. for their technical contributions, fruitful discussions, and encouragement.

■ REFERENCES

(1) Zhao, Y.; et al. Electrical spectroscopy of defect states and their hybridization in monolayer MoS_2. *Nat. Commun.* **2023**, *14*, 44.
(2) Kim, J. Y.; Gelczuk, Ł.; Polak, M. P.; Hlushchenko, D.; Morgan, D.; Kudrawiec, R.; Szlufarska, I. Experimental and theoretical studies of native deep-level defects in transition metal dichalcogenides. *npj 2D Mater. Appl.* **2022**, *6*, 75.
(3) Santosh, K. C.; Longo, R. C.; Addou, R.; Wallace, R. M.; Cho, K. Impact of intrinsic atomic defects on the electronic structure of MoS_2 monolayers. *Nanotechnology* **2014**, *25*, No. 375703.
(4) Lu, C.-P.; Li, G.; Mao, J.; Wang, L.-M.; Andrei, E. Y. Bandgap, mid-gap states, and gating effects in MoS_2. *Nano Lett.* **2014**, *14*, 4628–4633.
(5) Komsa, H.-P.; Krasheninnikov, A. V. Native defects in bulk and monolayer MoS_2 from first principles. *Phys. Rev. B* **2015**, *91*, No. 125304.
(6) Zhou, W.; et al. Intrinsic Structural Defects in Monolayer Molybdenum Disulfide. *Nano Lett.* **2013**, *13*, 2615–2622.
(7) Hötger, A.; et al. Spin-defect characteristics of single sulfur vacancies in monolayer MoS_2. *npj 2D Mater. Appl.* **2023**, *7*, 30.
(8) Nanet, H.; et al. Strong Photoluminescence Enhancement of MoS_2 through Defect Engineering and Oxygen Bonding. *ACS Nano* **2014**, *8*, 5738–5745.
(9) Mitterreiter, E.; et al. The role of chalcogen vacancies for atomic defect emission in MoS_2. *Nat. Commun.* **2021**, *12*, 3822.
(10) Vancsó, P.; Magda, G. Z.; Pető, J.; Noh, Ji-Y; Kim, Y.-S.; Hwang, C.; Biró, L. P.; Tapasztó, L. The intrinsic defect structure of exfoliated MoS_2 single layers revealed by Scanning Tunneling Microscopy. *Sci. Rep.* **2016**, *6*, 29726.
(11) Song, S. H.; et al. Probing defect dynamics in monolayer MoS_2 via noise nanospectroscopy. *Nat. Commun.* **2017**, *8*, 2121.
(12) Sangwan, V. K.; Arnold, H. N.; Jariwala, D.; Marks, T. J.; Lauhon, L. J.; Hersam, M. C. Low-Frequency Electronic Noise in Single-Layer MoS_2 Transistors. *Nano Lett.* **2013**, *13*, 4351–4355.
(13) Hooge, F. N. l/f Noise Sources. *IEEE Transaction on Electron Devices* **1994**, *41*, 1926.
(14) Marinari, E.; Parisi, G.; Ruelle, D.; Windey, P. On the Interpretation of $1/f$ Noise. *Commun. Math. Phys.* **1983**, *89*, 1–12.
(15) Grasser, T. *Noise in nanoscale semiconductor devices*; Springer, 2020.
(16) Palenskis, V.; Maknys, K. Nature of low-frequency noise in homogeneous semiconductors. *Sci. Rep.* **2015**, *5*, 18305.
(17) Waldherr, G.; Neumann, P.; Huelga, S. F.; Jelezko, F.; Wrachtrup, J. Violation of a temporal bell inequality for single spins in a diamond defect center. *Phys. Rev. Lett.* **2011**, *107*, No. 090401.
(18) Shields, B. J.; Unterreithmeier, Q. P.; de Leon, N. P.; Park, H.; Lukin, M. D. Efficient readout of a single spin state in diamond via spin-to-charge conversion. *Phys. Rev. Lett.* **2015**, *114*, No. 136402.
(19) Irber, D. M.; et al. Robust all-optical single-shot readout of nitrogen-vacancy centers in diamond. *Nat. Commun.* **2021**, *12*, 532.
(20) Kuhlmann, A. V.; et al. Charge noise and spin noise in a semiconductor quantum device. *Nat. Phys.* **2013**, *9*, 570.
(21) Wuetz, B. P.; et al. Reducing charge noise in quantum dots by using thin silicon quantum wells. *Nat. Commun.* **2023**, *14*, 1385.
(22) Sadegh, S.; Barkai, E.; Krapf, D. $1/f$ noise for intermittent quantum dots exhibits nonstationarity and critical exponent. *New J. Phys.* **2014**, *16*, No. 113054.
(23) Yang, Y.-C.; Coppersmith, S. N.; Friesen, M. Achieving high-fidelity single-qubit gates in a strongly driven charge qubit with $1/f$ charge noise. *npj Quantum Inf.* **2019**, *5*, 12.
(24) Mickelsen, D. L.; Carruzzo, H. M.; Yu, C. C. Interacting two-level systems as a source of $1/f$ charge noise in quantum dot qubits. *Phys. Rev. B* **2023**, *108*, No. 195307.
(25) Peters, M. G.; Dijkhuis, J. I.; Molenkamp, L. W. Random telegraph signals and noise in a silicon quantum dot. *J. Appl. Phys.* **1999**, *86*, 1523–1526.
(26) Niemann, M.; Kantz, H.; Barkai, E. Fluctuations of $1/f$ Noise and the Low-Frequency Cutoff Paradox. *Phys. Rev. Lett.* **2013**, *110*, No. 140603.
(27) Katagiri, Y.; et al. Gate-tunable atomically thin lateral MoS_2 schottky junction patterned by electron beam. *Nano Lett.* **2016**, *6*, 3788–3794.
(28) Nagamine, Y.; et al. Optoelectronic properties of laser-beam-patterned few-layer lateral MoS_2 Schottky junctions. *Appl. Phys. Lett.* **2020**, *117*, No. 043101.
(29) Kosugi, M.; et al. Electrical hysteresis characteristics in photogenerated currents on laser-beam-derived in-plane lateral 1D MoS_2- Schottky junctions. *AIP Advances* **2022**, *12*, 105210.
(30) Borders, W. A.; Pervaiz, A. Z.; Fukami, S.; Camsari, K. Y.; Ohno, H.; Datta, S. Integer factorization using stochastic magnetic tunnel junctions. *Nature* **2019**, *573*, 390.
(31) Chicca, E.; Indiveri, G. A recipe for creating ideal hybrid memristive-CMOS neuromorphic processing systems. *Appl. Phys. Lett.* **2020**, *116*, 120501.
(32) Xu, R.; et al. Vertical MoS_2 double-layer memristor with electrochemical metallization as an atomic-scale synapse with switching thresholds approaching 100 mV. *Nano Lett.* **2019**, *19*, 2411–2417.